ACS OMEGA

http://pubs.acs.org/journal/acsodf

Article

Anthracenemethyl Glycosides as Supramolecular Synthons for Chiral Self-Assembly and as Probes in Cell Imaging

Anne George and Narayanaswamy Jayaraman*

Cite This: *ACS Omega* 2023, 8, 16927−16934

Read Online

ACCESS | Metrics & More | Article Recommendations | Supporting Information

ABSTRACT: Chiral self-assembly of molecules warrants optimal structural features of synthons that promote formation of such self-assembled structures. A polyaromatic moiety coupled with hydrophilic, chiral-rich carbohydrates leads to segmentation of the regions and the self-assembly to supramolecular structures. Thermodynamic stability is augmented further through chiral self-assembly of the molecules, and formation of the desired chiral supramolecular structures is achieved. In the present study, we develop anthracene glycosides as efficient synthons that, in aqueous solutions, undergo facile self-assembly and lead to chiral supramolecular structures. Anthracenemethyl *O*-glycosides, installed with mono- and disaccharides, are studied for their self-assembly properties. Emerging chiral structures follow the configuration of the attached sugar moiety. Monosaccharide D- and L-glycopyranoside-containing derivatives alternate between left- and right-handed chiral structures, respectively. Disaccharide-containing derivatives do not exhibit chirality, even when self-assembly occurred. Photochemical $[4\pi + 4\pi]$ cycloaddition occurs in the self-assembled structure in aqueous solution. Cell viability assay using HeLa cells shows above 80% viable cells at a concentration of 50 μM. Bioimaging assays reveal a significant imaging of HeLa cells for anthracenemethyl D-glucopyranoside; bright imaging was observed at the perinuclear region of the cells, suggestive of an active transport of the molecules through the cell membrane. D-Galactopyranoside and L-glucopyranoside-containing derivatives show weak imaging potencies.

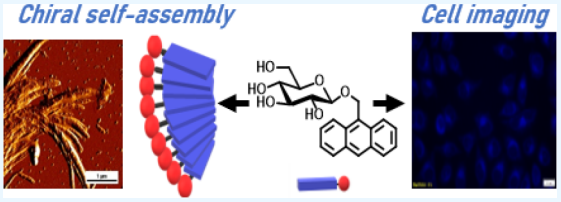

INTRODUCTION

Fluorophores conjugated with sugars offer the advantages of increased aqueous solubility, reduced cytotoxicity, and selectivity in cellular uptake.[1,2] Glycoconjugates possessing polyaromatic fluorophores are also known to self-assemble and form chiral supramolecular structures in aqueous solutions, as a result of the presence of a chiral-rich sugar moiety and emerging amphiphilicity.[3−13] Such glycoconjugates are found to be suitable in drug delivery[14,15] and imaging[16−19] and as multivalent ligands for proteins possessing specific sugar receptors.[20,21] A few prominent fluorophores in glycoconjugate studies are BODIPY,[22] 1,8-naphthalimide,[17] porphyrin,[9,10,23] perylene bisimide,[6−8] rhodamine,[18] tetraphenylethylene (TPE),[21] and pyrene.[19,24]

Bauerle and co-workers studied the chiral supramolecular structure formation in monosaccharide-conjugated oligothiophenes and observed that the sense of chirality was dependent on the configuration of the sugar. D- and L-mannose as the constituent in oligothiophene led the molecule to self-assemble and form left- and right-handed supramolecular stacks, respectively.[4] Studies by Liu and co-workers on perylene bisimide, appended with multiple carbohydrate moieties, demonstrated that the percentage of water content in aqueous solutions was sufficient to alternate between left- or right-handed chirality of the supramolecular structure.[6] A supramolecular chirality rule was also devised, depending on the carbohydrate moiety attached at the core.[7] Differences in the hydrogen bonding and steric effects were used to account for the changes in the stacking angle of the backbone. The nature of the linker also affected chirality in the supramolecular structure. Perylene bisimide modified with multiple mannose residues showed right-handed chirality when a triazole formed the linker, whereas the reverse left-handed chirality in the supramolecular structure was observed when an amide bond was used as the linker.[8] Functionalization of porphyrin at the meso-position with sugar moieties led to self-assembly in aqueous solutions, exhibiting a negative or positive bisignate band in the CD spectra, depending on the nature of the attached sugar.[9,10] The chiral self-assembly of the bolaamphiphilic sugar-terphenyl construct was demonstrated recently to form helical structures.[11] These studies illustrate that the overall chirality of the supramolecular structures possesses a direct correlation with the nature of the hydrophilic carbohydrate segment.

The use of anthracene as the aromatic core provides advantages in the self-assembly process, primarily due to its

Received: February 6, 2023
Accepted: March 27, 2023
Published: May 4, 2023

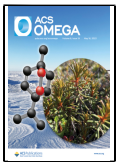

Scheme 1. Synthesis of 9-Anthracenemethyl Glycosides

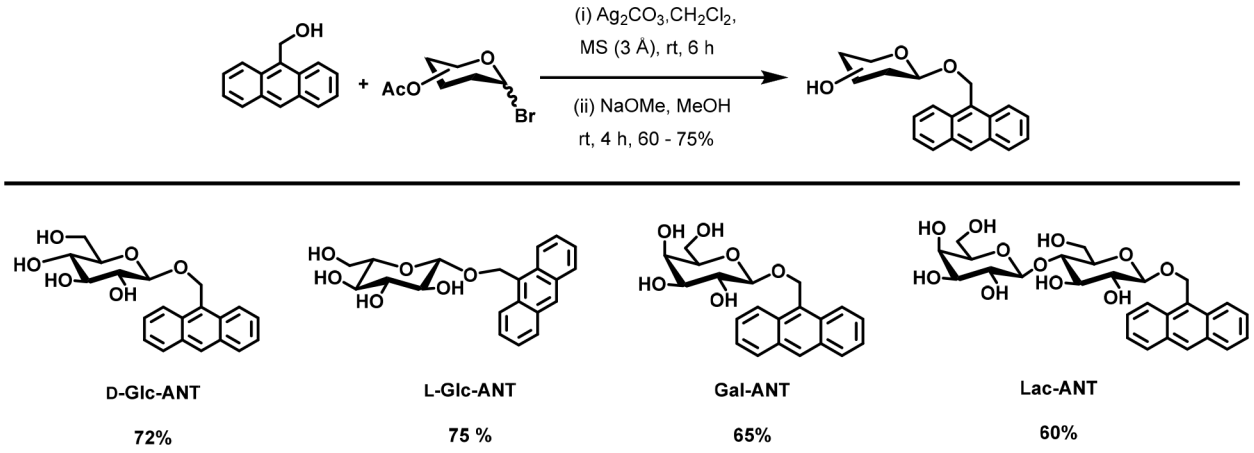

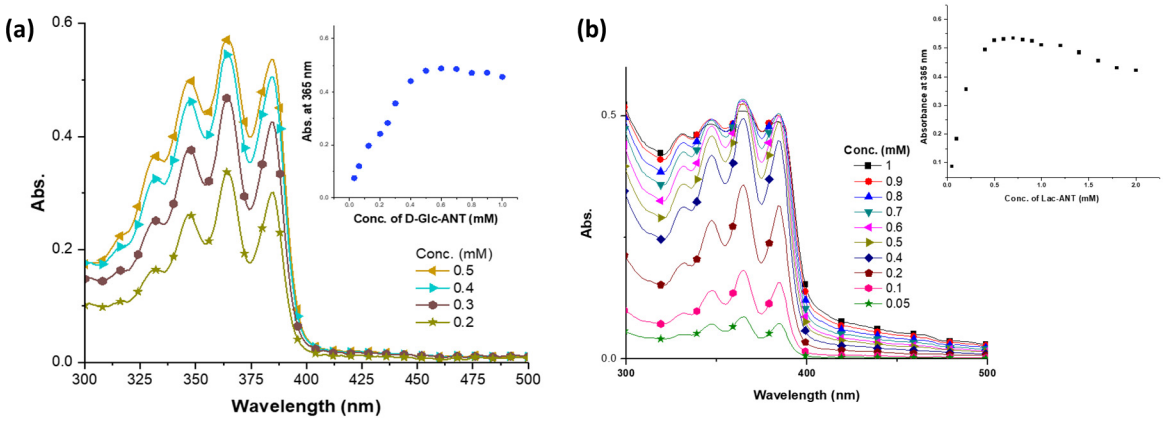

Figure 1. (a) UV−vis absorption spectra of D-Glc-ANT in aqueous solutions, [D-Glc-ANT] = 0.2−0.5 mM. Inset is a plot of the change in absorbance with the concentration of D-Glc-ANT. (b) UV−vis absorption spectra of **Lac-ANT** in aqueous solutions, [**Lac-ANT**] = 0.05−1.0 mM. Inset: plot of the change in absorbance with the concentration of **Lac-ANT**.

photophysical and photochemical properties. An early study by Iizawa and co-workers demonstrated the self-assembly of a thymidylic acid attached to an anthracene core in aqueous solutions. Self-assembly of the derivative occurred, to form helical J-aggregates when DNA was used as a template. Thymine−adenine base pair interaction induced a helical arrangement of the dipole moments along the anthracene short axis.[25] An achiral anthracene derivative, possessing a distal pyridinium ion attached via an alkyl linker, was found to self-assemble in the presence of an iodide anion to form chiral supramolecular structures.[26] Based on TEM analysis, it was suggested that the assembly process occurred through the initial formation of fibers and ribbons, which eventually led to twisted ribbons, responsible for the handedness. Molecular arrangement occurred with anthracene stacking and the positively charged pyridinium ions directed outside. Twisted ribbons shielded the hydrophobic core from the aqueous environment.

As a fluorophore, anthracene derivatives attract interest due to their optical properties of sharp absorption, emission bands, high quantum yields, photodimerization, and more.[27,28] It has a relatively higher excited state lifetime (τ_s = 5.3 ns) when compared to that of endogenous fluorophores in biological systems, thus reducing emission interference from biological molecules, such as amino acids and NAD(P)H.[29] However, aggregation-caused quenching and higher cellular cytotoxicity result in severely limited use of anthracene as a fluorophore in bioimaging studies. Natural products possessing an anthracene moiety covalently bound with carbohydrates act as radical scavengers and antibacterial agents.[30,31] Further, anthracene−carbohydrate hybrids, wherein a deoxyamino sugar is attached to an anthracene, function as fluorescent probes, as well as photocleaving agents of DNA and proteins.[32] A series of anthracene L-rhamnopyranosides were reported to show high cytotoxicity against cancer cells and DNA binding capacities, and the studies were conducted at μM concentrations.[33] The amphiphilic and chiral natures of these anthracene glycosides have not been exploited before in the self-assembly processes in aqueous solutions.

Stacking of the aromatic segment coupled with a chiral-rich hydrophilic sugar moiety has been found to provide an optimal route to develop defined chiral supramolecular structures. An investigation was undertaken to study the feasibility of anthracene−sugar conjugates as supramolecular synthons to favor formation of chiral supramolecular structures. Rich properties of the chromophore, coupled with reduced cytotoxicity arising from anthracene in such conjugates, would also permit biological studies where the chromophore acts as the probe. Synthesis of anthracene glycosides, possessing opposite configurations of the sugar moiety, their self-assembly behavior, and bioimaging properties in a cell line are disclosed herein. The study shows that the anthracene-

https://doi.org/10.1021/acsomega.3c00767
ACS Omega 2023, 8, 16927−16934

methyl glycosides of opposite configurations in the sugar segment undergo reversed chiral self-assemblies, above critical aggregation concentrations. Cytotoxicity profiles are assessed along with the bioimaging efficiency on a chosen cancer cell line.

RESULTS AND DISCUSSION

9-Anthracenemethyl glycosides are constituted of D- and L-glucose, galactose, and lactose that are attached to an anthracene core. The reaction of 9-hydroxymethyl anthracene with acetobromo sugars of D- and L-configurations, promoted by Ag_2CO_3, was used to synthesize the protected glycosides (Scheme 1). Removal of the acetyl groups under Zemplén conditions and subsequent purification afforded the anthracene glycosides D-Glc-ANT, L-Glc-ANT, **Gal-ANT** , and **Lac-ANT** in moderate yields. The glycosides are soluble in many organic solvents and in aqueous solutions. Structural homogeneities were verified by NMR spectroscopy and mass spectrometry.

A solution of D-Glc-ANT in DMSO showed two sets of bands in the UV−vis spectrum—an intense absorption in the 220−280 nm region corresponding to the $S_0 \rightarrow S_3$ transition and a vibronically structured band (320−400 nm) due to the $S_0\ ^1A_g \rightarrow S_1\ ^1B_{2u}$ transition.[34,35] In order to verify the aggregation of the molecule, the UV−vis spectrum of D-Glc-ANT was recorded in solution with varying proportions of DMSO and water. Solutions having a higher percentage of water led to a blue shift (2 nm) and a reduction in the absorbance intensities (Figure S9). **D-Glc-ANT** in aqueous solution showed an increase in absorbance with concentration until 0.5 mM (Figure 1a). Further increase of solution concentration led to a plateau in the absorption intensity, suggesting a critical aggregation concentration (CAC) of 0.5 mM. A similar trend was seen in the case of L-Glc-ANT in aqueous solution, with a plateau in absorbance above 0.5 mM (Figure S10). The UV−vis spectra of **Lac-ANT** in aqueous solution were also recorded to see the effect of a disaccharide on the aggregation of anthracene glycosides. From Figure 1b, a flattening of the peaks and a plateau in the absorption intensity are observed at concentrations higher than 0.5 mM, similar to that of D-Glc-ANT. Thus, for both monosaccharide as well as disaccharide anthracene conjugates, the CAC was found to be ∼0.5 mM.

The emission spectrum of **D-Glc-ANT** in DMSO solution showed three significant peaks at 397, 418, and 440 nm, similar to unfunctionalized anthracene in solution. The fluorescence of **D-Glc-ANT** in DMSO and H_2O mixed solutions showed a blue shift of 3 nm and a decrease in emission intensity with increasing water percentage, indicating the evolving $\pi-\pi$ stacking interactions as the water content increased (Figure S11). At increasing concentrations of D-Glc-ANT, the emission intensity in aqueous solutions began to plateau, from which the aggregation concentration was determined to be 0.5 mM (Figure 2), in agreement with that assessed by the UV−vis absorption spectrum.

The blue shift in absorbance and decrease in fluorescence in aqueous solutions at concentrations higher than 0.5 mM suggest that D-Glc-ANT forms an H-type aggregate, where the stacking direction of the monomers is perpendicular to the molecular plane.[36]

A circular dichroism study was undertaken to verify the formation of chiral aggregates. An aqueous solution of D-Glc-ANT (1 mM) showed a bisignate band with the crossover point at 253 nm, corresponding to the absorption of the anthracene moiety, whereas in DMSO solutions, no CD signal emerged (Figure S12). A positive Cotton peak and a negative Cotton peak were observed at 251 and 258 nm, respectively, suggesting an exciton coupling among the chromophores, as chiral self-assembly occurred in aqueous solutions. In order to verify how the configuration of sugar affects the chiral self-assembly, the CD of the L-glucose-attached anthracene glycoside, namely, L-Glc-ANT, was measured. The spectra of this opposite configuration anthracene glycoside emerged mirroring the spectrum recorded for **D-Glc-ANT** (Figure 3, left), with a comparatively lower intensity. The spectra corresponded to a left-handed chirality for **D-Glc-ANT**, whereas L-Glc-ANT corresponded to a right-handed chirality. The CD spectrum of a 1 mM solution of **Gal-ANT** showed a positive peak at 268 nm and a negative peak at 255 nm, with the intensity of the signal being weaker than that observed for glucose-attached anthracene (Figure 3, right). In the case of **Lac-ANT**, no significant CD signal was observed, indicating a lack of chirality in the aggregate formed.

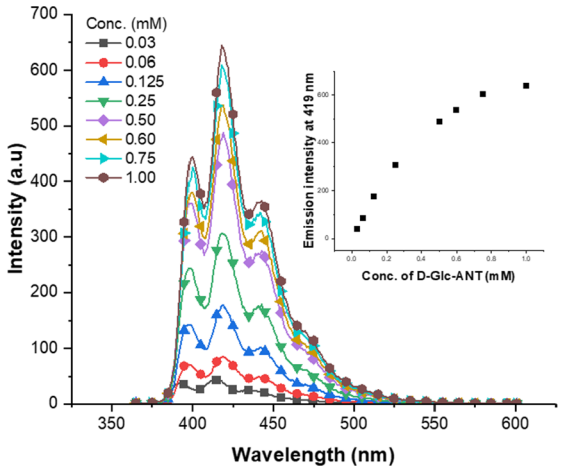

Figure 2. Emission spectra of an aqueous solution of D-Glc-ANT at varying concentrations of 0.0325−1 mM (λ_{ex} = 365 nm). Inset is a plot of the change in emission intensities at 419 nm with respect to the concentration.

The concentration-dependent CD study of D-Glc-ANT showed that the positive Cotton peak at 273 nm increased with increasing concentration, whereas a significant CD signal at 250 nm was observed only at concentrations above 0.6 mM (Figure 4). A shift of 3 nm in the bisignate CD signal was observed upon increasing the concentration from 0.8 to 1 mM. In the temperature-dependent study, a shift in the CD signal toward lower wavelengths was observed with increasing temperature due to a disturbance in the supramolecular chirality of the aggregate (Figure S13).

The morphologies of these amphiphiles were assessed further by AFM. Samples of **Glc-ANT** (aqueous solution) (1 mM) were prepared on a mica substrate and dried for 48 h. AFM images showed the morphology as bundles of twisted fibers for D-Glc-ANT. Similarly, in the case of **Gal-ANT**, fibers were observed while **Lac-ANT** appeared to form more particle-like aggregates rather than fibers, which explains the lack of an intense signal in the CD spectra (Figure 5a−c). Further, the corresponding SEM images showed the formation of the fiberlike structures for both the D- and L-forms of **Glc-ANT** (Figure 5d and e).

Based on the spectral data, the self-assembly of monomers to form H-aggregates, with the molecules arranged cofacially due

https://doi.org/10.1021/acsomega.3c00767
ACS Omega 2023, 8, 16927−16934

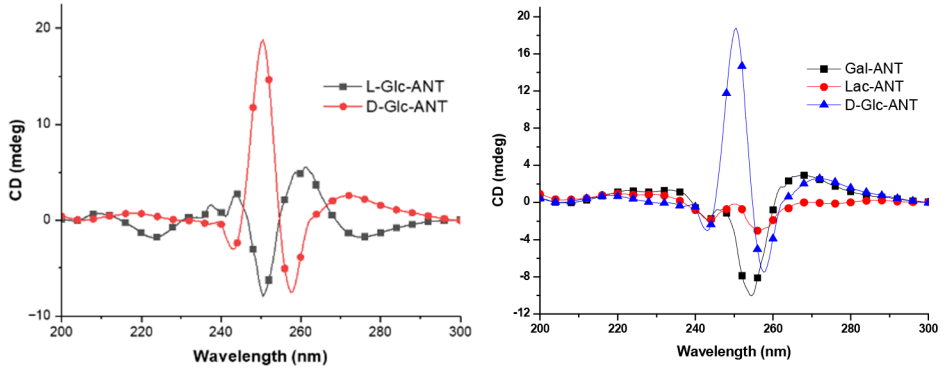

Figure 3. Left: CD spectrum of D-Glc-ANT and L-Glc-ANT in water, [**Glc-ANT**] = 1 mM. Right: CD spectra of D-Glc-ANT, **Gal-ANT**, and **Lac-ANT** (1 mM).

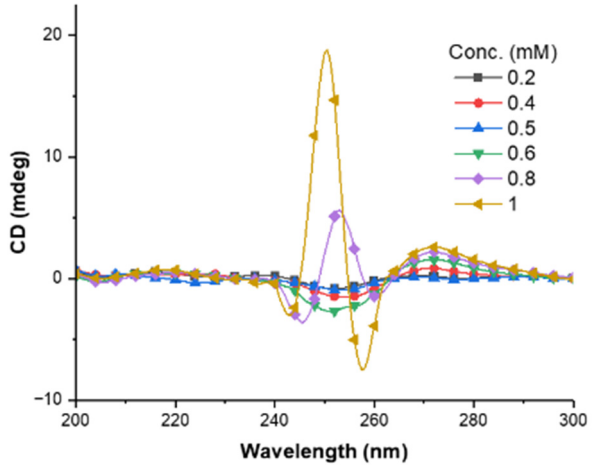

Figure 4. Concentration-dependent CD spectra of D-Glc-ANT in aqueous solution (0.2−1 mM).

to the $\pi-\pi$ stacking interactions of the anthracene unit but with a twist at each layer, is proposed to account for the supramolecular chirality (Figure 6).

Anthracene prominently undergoes [4π + 4π] photochemical reaction.[37] The photodimerization of D-Glc-ANT was assessed in aqueous solutions. An aqueous solution of D-Glc-ANT (1 mM) was irradiated at 365 nm, and the change in absorbance was recorded at periodic intervals (Figure 7). The broad absorbance in the 320−400 nm region disappeared upon continuous irradiation, suggesting the photoreaction of D-Glc-ANT. The mass spectrum (ESI-MS) showed the evolution of a small peak corresponding to that of the photodimer. The circular dichroism spectrum of the solution was devoid of Cotton peaks. The SEM images showed the presence of broken fiberlike structures (Figure 7, inset). An effort was undertaken to reverse the photoreaction by irradiation of the sample at 254 nm. However, neither this irradiation nor heating of the solution showed the retroreaction.

Preliminary biochemical studies were undertaken to assess the cytotoxicity and bioimaging properties of anthracene glycosides. In this study, HeLa cells were incubated with solutions of D-Glc-ANT, L-Glc-ANT, and **Gal-ANT** (20 μM) for 3 h. In the case of D-Glc-ANT, when the cells were viewed using the DAPI filter, significant fluorescence was observed, with the intensity concentrated in the perinuclear region (Figure 8a). The observed fluorescence was weaker in the case

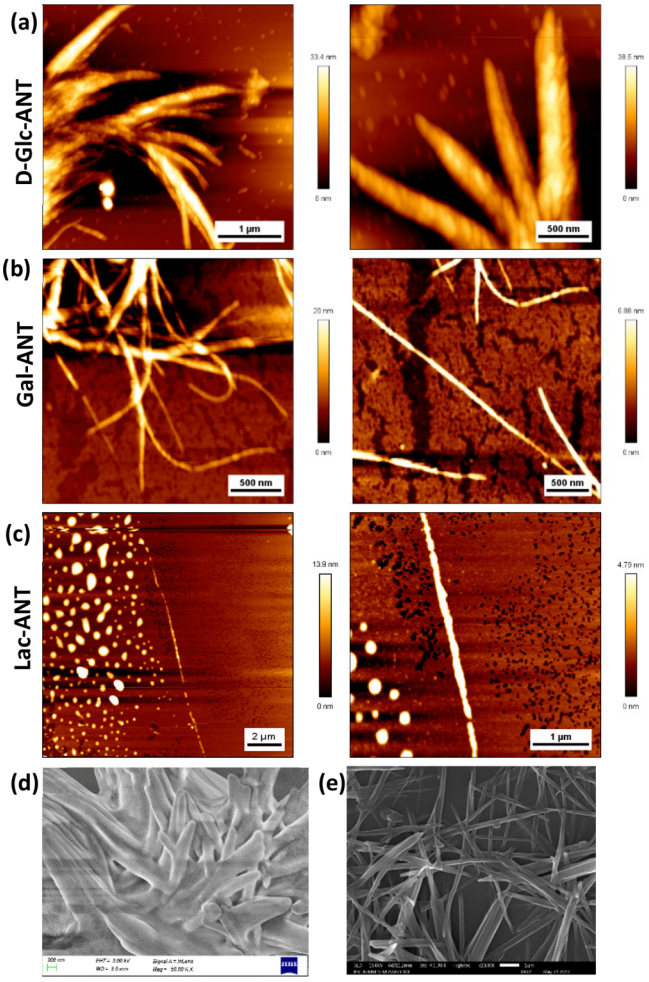

Figure 5. AFM images of (a) D-Glc-ANT (1 mM), (b) **Gal-ANT** (1 mM), and (c) **Lac-ANT** (0.75 mM); (d) SEM image of D-Glc-ANT (1 mM) (scale bar 200 nm); (e) SEM image of L-Glc-ANT (1 mM) (scale bar 1 μm).

of the cells incubated with **Gal-ANT** and L-Glc-ANT, indicating a lesser degree of uptake. The fluorescence intensity was quantified and was found to be lesser in the case of L-Glc-ANT (Figure 8b). Passive diffusion of the molecule through the cell membrane might be responsible for the observed fluorescence in the case of L-Glc-ANT. Cancer cells show increased uptake of glucose when compared to normal cells. The active transport of D-Glc-ANT through the membrane

https://doi.org/10.1021/acsomega.3c00767
ACS Omega 2023, 8, 16927−16934

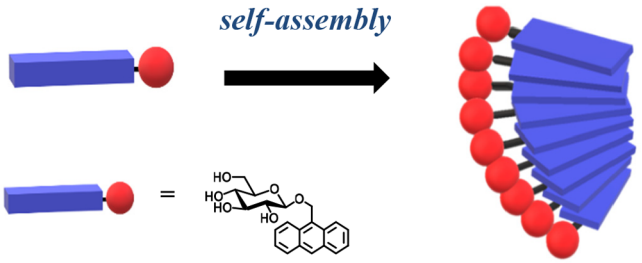

Figure 6. Proposed model of the self-assembly of D-Glc-ANT in aqueous solution.

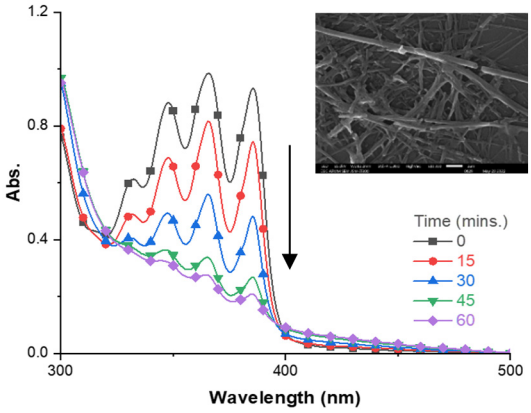

Figure 7. UV−vis spectrum of an aqueous solution of D-Glc-ANT (1 mM) upon irradiation at 365 nm. Inset is the SEM image of the irradiated solution of D-Glc-ANT (scale bar 1 μM).

might explain the stronger fluorescence observed for D-Glc-ANT. The cytotoxicity of D-Glc-ANT was assessed by incubating HeLa cells with varying concentrations of D-Glc-ANT (10−50 μM) for 24 h. The percentage cell viability was determined by MTT assay. D-Glc-ANT was not toxic to the cells even at higher concentrations, with the percentage of cell viability staying above 80% (Figure 8c). This opens up the possibility for the potential application of these compounds for photodynamic therapy (PDT) due to the known phototoxicity of anthracene.[38]

CONCLUSION

Anthracenemethyl glycosides are studied as effective supramolecular synthons, permitting formation of chiral self-assembled structures. 9-Anthracenemethyl glycosides undergo self-assembly in aqueous solutions to form chiral aggregates at concentrations above 0.5 mM. The $\pi-\pi$ stacking of the anthracene core drives the self-assembly process, in combination with the hydrophilic carbohydrate moieties. The chirality of the self-assembled structure is dependent on the nature of the carbohydrate moiety. AFM and SEM characterizations reveal fiberlike structures. The self-assembled structure is irreversibly disrupted upon irradiation at 365 nm, due to the photoreaction of anthracene. The emission of the anthracene moiety also permits studies of anthracenyl glycosides in cellular uptake. Reduced cytotoxicity of the anthracene as a result of conjugation with carbohydrates, coupled with sugar-dependent selectivity in cellular uptake, enables facile imaging of cells. Further studies might find applications of these molecules for photodynamic therapy due to the known phototoxicity of anthracene and its byproducts.

EXPERIMENTAL SECTION

General Methods. Solvents were dried and distilled according to literature procedures. All chemicals were purchased from commercial sources and were used without further purification. Silica gel (100−200 and 230−400 mesh) was used for column chromatography, and TLC analysis was performed on commercial plates coated with silica gel 60 F254. Visualization of the spots on TLC plates was achieved by UV radiation or spraying 5% sulfuric acid in ethanol. High-resolution mass spectra were obtained from the Q-TOF instrument by electrospray ionization (ESI). ^{1}H and ^{13}C NMR spectral analyses were performed on a spectrometer operating at 400 and 100 MHz, respectively. Chemical shifts are reported with respect to tetramethyl silane (TMS) for ^{1}H NMR and the central line (49.00 ppm) of CD_3OD for ^{13}C NMR analyses.

Steady-state absorption and fluorescence measurements were performed on an UV−vis spectrophotometer and a fluorescence spectrometer, with 2.5 nm slit width at excitation and 5 nm slit width at emission monochromators. A circular dichroism spectrometer was used for CD measurements, a quartz cuvette 0.2 mm path length was used, and the sample chamber was flushed with N_2 (g) during analysis.

AFM studies were conducted on an instrument, using built-in software for the analysis. In order to visualize the shape and morphology, freshly prepared aqueous solutions of D-Glc-ANT were drop-cast on a freshly cleaved mica substrate. The images were acquired in tapping mode at a scanning rate of 1.0 Hz. The typical resonant frequency of AFM tips was 300 kHz, and the force constant of the cantilever was 40 N/m. The samples were analyzed by FESEM, and images were captured in GBH mode with the accelerating voltage of 0.7 kV and working distance of 4 mm. A secondary electron imaging detector was used. Fluorescence imaging of the cells was performed using an inverted microscope and DAPI-5060C-000 BrightLine single-band filter (excitation 352−402 nm, emission 417−477 nm). Fluorescence intensity was quantified using ImageJ software. Absorbance of the 96-well plate was recorded using a multimode microplate reader (λ_{max} 570 nm).

Synthesis of Anthracenemethyl Glycosides. Activated molecular sieves (3 Å) were added to a solution of acetobromo glucose (1 molar equiv) and 9-anthracene methanol (1.5 molar equiv) in freshly distilled CH_2Cl_2. Ag_2CO_3 (1 molar equiv) was added to the reaction mixture in the dark, and the reaction mixture was stirred for 6 h at room temperature. The crude reaction mixture was filtered through a Celite pad and concentrated *in vacuo*. It was redissolved in MeOH, and a solution of NaOMe in MeOH was added dropwise until a pH of 14 was obtained. After 4 h, the reaction mixture was neutralized with Amberlite resin, filtered, and concentrated *in vacuo*. The crude reaction mixture was purified by column chromatography (100−200 mesh SiO_2) in a $CHCl_3$/MeOH linear gradient to afford the anthracenemethyl glycosides. The anthracenemethyl glycosides were characterized by ^{1}H, ^{13}C NMR, and HRMS techniques.

Anthracen-9-ylmethyl β-D-Glucopyranoside (D-Glc-ANT). Yield: 72%. $[\alpha]_D$ −6.00 (c = 1, CH_3OH). ^{1}H NMR (CD_3OD, 400 MHz): δ 8.56 (d, J = 8 Hz, 2H), 8.52 (s, 1H), 8.04 (d, J = 8 Hz, 2H), 7.58−7.54 (m, 2H), 7.50−7.48 (m, 2H), 5.82 (quartet, J = 12 Hz, 2H), 4.43 (d, J = 8 Hz, 1H), 4.00 (dd, J = 12 Hz, 2 Hz, 1H), 3.79 (dd, J = 12 Hz, 6 Hz, 2H), 3.35−3.33 (m, 1H), 3.28−3.22 (m, 2H). ^{13}C NMR (CD_3OD, 100 MHz) δ 132.9, 132.7, 129.9, 129.6, 129.1, 127.4, 126.1, 125.8, 102.8,

https://doi.org/10.1021/acsomega.3c00767
ACS Omega 2023, 8, 16927−16934

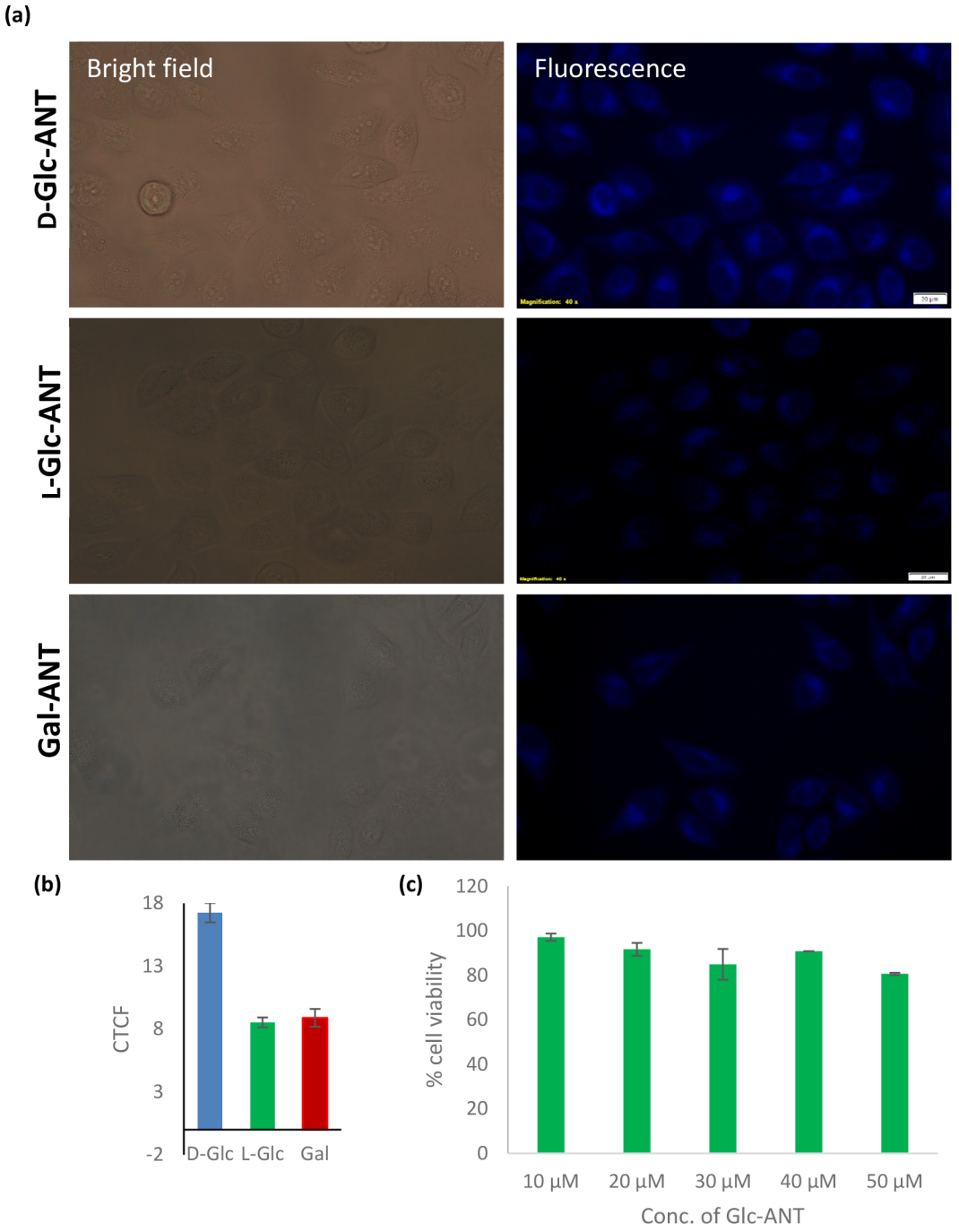

Figure 8. (a) Uptake of anthracenemethyl glycosides by HeLa cells observed with an inverted microscope, using the DAPI filter (scale bar 20 μM). HeLa cells were incubated with 20 μM of the anthracenemethyl glycosides for 3 h. (b) Quantified fluorescence intensity (CTCF) of D- (blue bar) and L-Glc-ANT (green bar) and **Gal-ANT** (red bar). (c) Concentration-dependent cytotoxicity study of D-Glc-ANT upon incubation with HeLa cells for 24 h.

78.2, 78.0, 75.0, 71.8, 63.5, 62.9. ESI-MS m/z: $[M + Na]^+$ calcd. for $C_{21}H_{22}O_6Na$ = 393.1314; found 393.1315.

Anthracen-9-ylmethyl β-L-Glucopyranoside (L-Glc-ANT). Yield: 75%. $[\alpha]_D$ +6.48 (c = 0.5, CH_3OH). ^1H NMR (CD_3OD, 400 MHz): δ 8.58−8.54 (m, 3H), 8.05 (d, J = 8 Hz, 2H), 7.59−7.56 (m, 2H), 7.51−7.48 (m, 2H), 5.83 (quartet, J = 12 Hz, 2H), 4.45 (d, J = 7.2 Hz, 1H), 4.01 (dd, J = 11.8 Hz, 1.6 Hz, 1H), 3.80 (dd, J = 11.8 Hz, 6 Hz, 1H), 3.71−3.65 (m, 1H), 3.36−3.34 (m, 1H), 3.27−3.21 (m, 2H). ^{13}C NMR (CD_3OD, 100 MHz) δ 132.9, 132.8, 129.9, 129.6, 129.1, 127.4, 126.1, 125.8, 102.8, 78.2, 78.1, 75.0, 71.8, 63.6, 63.0. ESI-MS m/z: $[M + Na]^+$ calcd. for $C_{21}H_{22}O_6Na$ = 393.1314; found 393.1311.

*Anthracen-9-ylmethyl β-D-Galactopyranoside (**Gal-ANT**).* Yield: 65%. ^1H NMR (CD_3OD, 400 MHz): δ 8.55 (d, J = 8 Hz, 2H), 8.51 (s, 1H), 8.03 (d, J = 8 Hz, 2H), 7.56−7.53 (m, 2H), 7.49−7.45 (m, 2H), 5.80 (AB quartet, J = 12 Hz, 2H), 4.40 (d, J = 8 Hz, 1H), 3.93−3.88 (m, 1H), 3.83−3.80 (m, 2H), 3.57−3.52 (m, 2H), 3.39−3.36 (m, 1H). ^{13}C NMR (CD_3OD, 100 MHz) δ 132.9, 132.7, 129.9, 129.5, 129.2, 127.3, 126.1, 125.9, 103.5, 76.9, 74.9, 72.4, 70.4, 63.5, 62.6.

https://doi.org/10.1021/acsomega.3c00767
ACS Omega 2023, 8, 16927−16934

ESI-MS m/z: $[M + Na]^+$ calcd. for $C_{21}H_{22}O_6Na$ = 393.1314; found 393.1312.

*Anthracen-9-ylmethyl β-D-Galactopyranosyl-(1 → 6)-β-D-glucopyranoside (**Lac-ANT**).* Yield: 60%. ^1H NMR (CD_3OD, 400 MHz): δ 8.54−8.52 (m, 3H), 8.03 (d, J = 8 Hz, 2H), 7.56−7.53 (m, 2H), 7.48−7.45 (m, 2H), 5.80 (AB quartet, J = 12 Hz, 2H), 4.43 (d, J = 8 Hz, 1H), 4.35 (d, J = 8 Hz, 1H), 4.02 (dd, J_1 = 12 Hz, J_2 = 4 Hz, 1H), 3.92 (dd, J_1 = 12 Hz, J_2 = 4 Hz, 1H), 3.79−3.71 (m, 3H), 3.68−3.62 (m, 3H), 3.58−3.53 (m, 2H), 3.49−3.37 (m, 2H). ^{13}C NMR (CD_3OD, 100 MHz) δ 132.9, 132.7, 129.9, 129.7, 129.0, 127.4, 126.1, 125.8, 105.1, 102.7, 80.7, 77.1, 76.7, 76.4, 74.8, 74.6, 72.6, 70.3, 63.7, 62.5, 62.1. ESI-MS m/z: $[M + Na]^+$ calcd. for $C_{27}H_{32}O_{11}Na$ = 555.1842; found 555.1840.

Cell Culture. HeLa cells were grown in T-25 flasks (NEST) using DMEM high-glucose media (Himedia), supplemented with 10% fetal bovine serum (Himedia), antibiotic antimycotic solution (10 μL), and phenol red as an indicator. The cells were incubated at 37 °C with 5% CO_2.

Toxicity Studies. HeLa cells were seeded at a density of 10^4 cells/well with 100 μL of DMEM media per well in a 96-well plate and cultured overnight. The media were discarded, and the wells were washed with 1 × PBS solution. Aqueous solutions of D-Glc-ANT at varying concentrations (10−50 μM) were loaded, with each concentration in triplicate, while untreated cells were used as the blank. It was incubated for 24 h, the media were discarded, and a solution of MTT in PBS (100 μL) (0.5 mg mL^{-1}) was added to each well. After incubation for 3 h in the dark, the formazan formed was dissolved in DMSO, and the absorbance at 570 nm was measured for each well. The average absorbance for each concentration was calculated and used to determine the cell viability, with the formula of % cell viability as $(Abs_{sample} - Abs_{blank}/Abs_{untreated}) \times 100$. Experiments were performed twice, and the average percentage cell viability was plotted with the standard error calculated using the formula std. error = $\sigma/\sqrt{n}$, where σ = std. deviation and n = sample size.[39]

Cellular Uptake. HeLa cells were seeded on 40.4 mm Nunc glass bottom dishes and left overnight. The media were discarded, and the cells were washed with PBS (1 mL). Solutions of anthracenemethyl glycosides (20 μM) were loaded onto the dish and left to incubate for 3 h. The cells were washed with PBS (2 × 1 mL). The cells were immersed in PBS (1 mL) and observed under a fluorescence microscope using a DAPI filter.

■ ASSOCIATED CONTENT

Supporting Information

The Supporting Information is available free of charge at https://pubs.acs.org/doi/10.1021/acsomega.3c00767.

^1H and ^{13}C NMR spectra of compounds, UV−vis spectra, emission spectra, and circular dichroism spectra (PDF)

■ AUTHOR INFORMATION

Corresponding Author

Narayanaswamy Jayaraman − *Department of Organic Chemistry, Indian Institute of Science, Bangalore 560012, India;* orcid.org/0000-0001-5577-8053; Email: jayaraman@iisc.ac.in

Author

Anne George − *Department of Organic Chemistry, Indian Institute of Science, Bangalore 560012, India*

Complete contact information is available at: https://pubs.acs.org/10.1021/acsomega.3c00767

Author Contributions

The manuscript was written through the contributions of all authors. All authors have given approval to the final version of the manuscript.

Notes

The authors declare no competing financial interest.

■ ACKNOWLEDGMENTS

We thank SERB-DST, New Delhi, for financial support. A.G. acknowledges the CSIR, New Delhi, for a research fellowship.

■ ABBREVIATIONS

CD: circular dichroism; TLC: thin-layer chromatography; MTT: 3-(4,5-dimethylthiazol-2-yl)-2,5-diphenyltetrazolium bromide; PBS: phosphate-buffered saline; DAPI: 4′,6-diamidino-2-phenylindole

■ REFERENCES

(1) (a) Thomas, B.; Yan, K. C.; Hu, X. L.; Donnier-Marechal, M.; Chen, G. R.; He, X. P.; Vidal, S. Fluorescent Glycoconjugates and Their Applications. *Chem. Soc. Rev.* **2020**, *49*, 593−641. (b) Chabre, Y. M.; Roy, R. Multivalent Glycocoonjugate Syntheses and Applications Using Aromatic Scaffolds. *Chem. Soc. Rev.* **2013**, *42*, 4657−4708.

(2) He, X. P.; Zang, Y.; James, T. D.; Li, J.; Chen, G. R.; Xie, J. Fluorescent Glycoprobes: A Sweet Addition for Improved Sensing. *Chem. Commun.* **2017**, *53*, 82−90.

(3) Brito, A.; Abul-Haija, Y. M.; da Costa, D. S.; Novoa-Carballal, R.; Reis, R. L.; Ulijn, R. V.; Pires, R. A.; Pashkuleva, I. Minimalistic Supramolecular Proteoglycan Mimics by Co-Assembly of Aromatic Peptide and Carbohydrate Amphiphiles. *Chem. Sci.* **2019**, *10*, 2385−2390.

(4) Schmid, S.; Mena-Osteritz, E.; Kopyshev, A.; Bauerle, P. Self-Assembling Carbohydrate-Functionalized Oligothiophenes. *Org. Lett.* **2009**, *11*, 5098−5101.

(5) Michel, S. S. E.; Kilner, A.; Eloi, J. C.; Rogers, S. E.; Briscoe, W. H.; Galan, C. Norbornene-Functionalized Chitosan Hydrogels and Microgels via Unprecedented Photoinitiated Self-Assembly for Potential Biomedical Applications. *ACS Appl. Bio Mater.* **2020**, *3*, 5253−5262.

(6) Wang, K. R.; An, H. W.; Wang, Y. Q.; Zhang, J. C.; Li, X. L. Multivalent Glycoclusters Constructed by Chiral Self-Assembly of Mannose Functionalized Perylene Bisimide. *Org. Biomol. Chem.* **2013**, *11*, 1007−1012.

(7) Wang, K. R.; Han, D.; Cao, G. J.; Li, X. L. Synthesis and Predetermined Supramolecular Chirality of Carbohydrate-Functionalized Perylene Bisimide Derivatives. *Chem.—Asian J.* **2015**, *10*, 1204−1214.

(8) Wang, K. R.; Han, D.; Cao, G. J.; Li, X. L. Link Spacer Controlled Supramolecular Chirality of Perylene Bisimide-Carbohydrate Conjugate. *RSC Adv.* **2015**, *5*, 47728−47731.

(9) Stepanek, P.; Dukh, M.; Saman, D.; Moravcova, J.; Kniezo, L.; Monti, D.; Venanzi, M.; Mancini, G.; Drasar, P. Synthesis and Solvent Driven Self-Aggregation Studies of *meso*-"C-Glycoside"- Porphyrin Derivatives. *Org. Biomol. Chem.* **2007**, *5*, 960−970.

(10) Monti, D.; Venanzi, M.; Gatto, E.; Mancini, G.; Sorrenti, A.; Stepanek, P.; Drasar, P. Study of the Supramolecular Chiral Assembly of *meso*-"C-Glucoside"- Porphyrin Derivatives in Aqueous Media. *New J. Chem.* **2008**, *32*, 2127−2133.

(11) Bag, K.; Naresh, K.; Jayaraman, N. Chiral Self-Assembly of Bolaamphiphilic Sugar-Terphenyl-Sugar Constructs. *Mater. Today Chem.* **2022**, *26*, 101026.
(12) Peters, K. C.; Mekala, S.; Gross, R. A.; Singer, K. D. Cooperative Self-Assembly of Helical Exciton-Coupled Biosurfactant-Functionalized Porphyrin Chromophores. *ACS Appl. Bio Mater.* **2019**, *2*, 1703−1713.
(13) Lin, C.; Maisonneuve, S.; Metivier, R.; Xie, J. Photoswitchable Carbohydrate-Based Macrocyclic Azobenzene: Synthesis, Chiroptical Switching, and Multistimuli-Responsive Self-Assembly. *Chem.—Eur. J.* **2017**, *23*, 14996−15001.
(14) Cohen, Y.; Rutenberg, R.; Cohen, G.; Veltman, B.; Gvirtz, R.; Fallik, E.; Danino, D.; Eltzov, E.; Poverenov, E. Aminated Polysaccharide-Based Nanoassemblies as Stable Biocompatible Vehicles Enabling Crossing of Biological Barriers: An Effective Transdermal Delivery of Diclofenac Medicine. *ACS Appl. Bio Mater.* **2020**, *3* (4), 2209−2217.
(15) Cao, S.; Pei, Z.; Xu, Y.; Pei, Y. Glyco-Nanovesicles with Activatable Near-Infrared Probes for Real-Time Monitoring of Drug Release and Targeted Delivery. *Chem. Mater.* **2016**, *28*, 4501−4506.
(16) Liu, Y.; Ji, D. K.; Dong, L.; Galanos, N.; Zang, Y.; Li, J.; Vidal, S.; He, X. P. Supramolecular Assembly of Fluorogenic Glyco-Dots from Perylenediimide-Based Glycoclusters for Targeted Imaging of Cancer Cells. *Chem. Commun.* **2017**, *53*, 11937−11940.
(17) Calatrava-Perez, E.; Bright, S. A.; Achermann, S.; Moylan, C.; Senge, M. O.; Veale, E. B.; Williams, C.; Gunnlaugsson, T.; Scanlan, E. M. Glycosidase Activated Release of Fluorescent 1,8-Naphthalimide Probes for Tumor Cell Imaging from Glycosylated 'Pro-Probes'. *Chem. Commun.* **2016**, *52*, 13086−13089.
(18) Jo, A.; Lee, S.; Nam, H.; Lee, H. W.; Park, J.; Kim, H. M.; Kim, E.; Park, S. B.; Sung, J. Near-IR Fluorescent Tracer for Glucose-Uptake Monitoring in Live Cells. *Bioconjugate Chem.* **2018**, *29*, 3394−3401.
(19) Sun, Q.; Zhu, H. Y.; Wang, J. F.; Chen, X.; Wang, K. R.; Li, X. L. Supramolecular Nanofiber of Pyrene-Lactose Conjugates and its Two-Photon Fluorescence Imaging. *Bioorg. Chem.* **2018**, *79*, 126−130.
(20) Dou, W. T.; Zeng, Y. L.; Lv, Y.; Wu, J.; He, X. P.; Chen, G. R.; Tan, C. Supramolecular Ensembles Formed between Charged Conjugated Polymers and Glycoprobes for the Fluorogenic Recognition of Receptor Proteins. *ACS Appl. Mater. Interfaces* **2016**, *8*, 13601−13606.
(21) Donnier Marechal, M.; Abdullayev, S.; Bauduin, M.; Pascal, Y.; Fu, M. Q.; He, X. P.; Gillon, E.; Imberty, A.; Kipnis, E.; Dessein, R.; Vidal, S. Tetraphenylethylene-Based Glycoclusters with Aggregation-Induced Emission (AIE) Properties as High-Affinity Ligands of Bacterial Lectins. *Org. Biomol. Chem.* **2018**, *16*, 8804−8809.
(22) Uppal, T.; Bhupathiraju, D. K.; Vicente, M. G. H. Synthesis and Cellular Properties of Near-IR BODIPY−PEG and Carbohydrate Conjugates. *Tetrahedron* **2013**, *69*, 4687−4693.
(23) Daly, R.; Vaz, G.; Davies, A. M.; Senge, M. O.; Scanlan, E. M. Synthesis and Biological Evaluation of a Library of Glycoporphyrin Compounds. *Chem.—Eur. J.* **2012**, *18*, 14671−14679.
(24) Kanamori, T.; Matsuyama, A.; Naito, H.; Tsuga, Y.; Ozako, Y.; Ogura, S. I.; Okazaki, S.; Yuasa, H. Water-Soluble Glucosyl Pyrene Photosensitizers: An Intramolecularly Synthesized 2-*C*-Glucoside and an *O*-Glucoside. *J. Org. Chem.* **2018**, *83*, 13765−13775.
(25) Iwaura, R.; Ohnishi-Kameyama, M.; Iizawa, T. Construction of Helical J-Aggregates Self-Assembled from a Thymidylic Acid Appended Anthracene Dye and DNA as a Template. *Chem.—Eur. J.* **2009**, *15*, 3729−3735.
(26) Hu, J.; Gao, L.; Zhu, Y.; Wang, P.; Lin, Y.; Sun, Z.; Yang, S.; Wang, Q. Chiral Assemblies from an Achiral Pyridinium-Tailored Anthracene. *Chem.—Eur. J.* **2017**, *23*, 1422−1426.
(27) Turro, N. J.; Ramamurthy, V.; Scaiano, J. C. *Modern Molecular Photochemistry of Organic Molecules*; University Science Books: Melville, NY, 2010.
(28) Sonnenschein, M.; Amirav, A.; Jortner, J. Absolute Fluorescence Quantum Yields of Large Molecules in Supersonic Expansions. *J. Phys. Chem.* **1984**, *88*, 4214−4218.
(29) Berezin, M. Y.; Achilefu, S. Fluorescence Lifetime Measurements and Biological Imaging. *Chem. Rev.* **2010**, *110*, 2641−2684.
(30) Li, Y.; Li, X.; Lee, U.; Kang, J. S.; Choi, H. D.; Sona, B. W. A New Radical Scavenging Anthracene Glycoside, Asperflavin Ribofuranoside, and Polyketides from a Marine Isolate of the Fungus Microsporum. *Chem. Pharm. Bull.* **2006**, *54*, 882−883.
(31) Tung, N. H.; Ding, Y.; Choi, E. M.; Van Kiem, P.; Van Minh, C.; Kim, Y. H. New Anthracene Glycosides from *Rhodomyrtus Tomentosa* Stimulate Osteoblastic Differentiation of MC3T3-E1 Cells. *Arch Pharm. Res.* **2009**, *32*, 515−520.
(32) Hasegawa, M.; Suzuki, A.; Matsumura, S.; Toshima, K. Molecular Design, Chemical Synthesis, and Evaluation of Novel Anthracene Derivatives as a New Family of Protein Photocleavers. *Sci. Technol. Adv. Mater.* **2006**, *7*, 169−174.
(33) Song, G.; Liu, H.; Zhang, W.; Geng, M.; Li, Y. Synthesis and Biological Evaluation of Cytotoxic Activity of Novel Anthracene L-Rhamnopyranosides. *Bioorg. Med. Chem.* **2010**, *18*, 5183−5193.
(34) Zilberg, S.; Samuni, U.; Fraenkel, R.; Haas, Y. The Vibrational Structure of the $S_0 \rightarrow S_1$ Transition of Anthracene. *Chem. Phys.* **1994**, *186*, 303−316.
(35) Baba, M.; Saitoh, M.; Taguma, K.; Shinohara, K.; Yoshida, K.; Semba, Y.; Kasahara, S.; Nakayama, N.; Goto, H.; Ishimoto, T.; Nagashima, U. Structure and Excited-State Dynamics of Anthracene: Ultrahigh-Resolution Spectroscopy and Theoretical Calculation. *J. Chem. Phys.* **2009**, *130*, 134315.
(36) (a) Ma, S.; Du, S.; Pan, G.; Dai, S.; Xu, B.; Tian, W. Organic Molecular Aggregates: From Aggregation Structure to Emission Property. *Aggregate* **2021**, *2* (4), e96. (b) Lubtow, M.; Helmers, I.; Stepanenko, V.; Albuquerque, R. Q.; Marder, T. B.; Fernandez, G. Self-Assembly of 9,10-Bis(phenylethynyl) Anthracene (BPEA) Derivatives: Influence of π- π and Hydrogen-Bonding Interactions on Aggregate Morphology and Self-Assembly Mechanism. *Chem.—Eur. J.* **2017**, *23*, 6198−6205.
(37) Bouas-Laurent, H.; Castellan, A.; Desvergne, J. P.; Lapouyade, R. Photodimerization of Anthracenes in Fluid Solutions: (Part 2) Mechanistic Aspects of the Photocycloaddition and of the Photochemical and Thermal Cleavage. *Chem. Soc. Rev.* **2001**, *30*, 248−263.
(38) Takagi, R.; Takeda, A.; Takahashi, D.; Toshima, K. Target-Selective Fluorescence Imaging and Photocytotoxicity against H_2O_2 High-Expressing Cancer Cells Using a Photoactivatable Theranostic Agent. *Chem.—Asian J.* **2017**, *12*, 2656−2659.
(39) van Meerloo, J.; Kaspers, G. J. L.; Cloos, J. Cell Sensitivity Assays: The MTT Assay. *Methods Mol. Biol.* **2011**, *731*, 237−245.

https://doi.org/10.1021/acsomega.3c00767
ACS Omega 2023, 8, 16927−16934